Experiments in Fluids 27 (1999) 181–188 © Springer-Verlag 1999

Influence of precession on velocity measurements in a strong laboratory vortex

R. Wunenburger, B. Andreotti, P. Petitjeans

Abstract A strong laboratory vortex is generated in a cylindrical cell using a rotating disk and stretched by pumping the fluid out through a hole in the centre of the top of the cell. The velocity field is measured by means of laser Doppler anemometry and Doppler ultrasonic anemometry which are both non intrusive methods. The vortex exhibits a slight precession which induces temporal fluctuations of the velocity at the measurement point. Due to the centrifugal force, the tracers concentrate in a tubular region around the vortex, leading to spatial variations of the measurement counting rate. Under these two effects, the probability density function (PDF) of the one point velocity exhibits a strong non-Gaussian behaviour. In order to access the details of the velocity profile of the vortex in its own system of reference, the influence of the vortex precession, of the spatial variations of the concentration in tracers and of the intrinsic measurement dispersion is investigated and a model is proposed. It allows to recover statistically the characteristics of the vortex and to deduce the trajectory of its centre from the instantaneous velocity profiles.

1 Introduction

In this paper some experimental problems encountered while characterising the velocity field of a strong stretched vortex are discussed. Since a vortex is very sensitive to perturbations, non intrusive methods have to be used (both laser Doppler anemometry (LDA) and Doppler ultrasonic anemometry (DUA) in our case). Due to the poor spatial resolution of these methods, the difficulty is to perform measurements in flows exhibiting strong velocity gradients, and in the particular case of a vortex, to get a close look to the details of the vortex core. Moreover, the precession of the vortex and the spatial variations of the tracer concentration lead to large fluctuations of the measurements and to a systematic gap between the averaged velocity and the instantaneous velocity in the vortex frame of reference. A method is discussed based on the analysis of the velocity PDFs allowing to overcome these difficulties. Since this kind of measurement problems are frequently encountered, the study presented here on the particular case of a precessing vortex should be seen as an applied example of a general statistical treatment of velocity measurements.

Several configurations have been previously used to produce vortices. All these methods are somehow based on the principle of the bathtube vortex. The main way of creating a strong isolated vortex is to provide some means of producing angular momentum and of concentrating it by an inflow towards the centre of rotation. A classical issue to produce circulation has been to use a rotating tank (Turner 1966; Mory and Yurchenko 1993), a rotating disk in a fixed cylindrical tank (Escudier 1984; Mory and Spohn 1992), or two co-rotating disks (Pinton and Labbe 1994). Escudier (1984) and Mory and Spohn (1992) used the toroidal secondary flow created by Eckman layer suction to stretch the vortex: in this geometry, a central flat unstable vortex is formed which encounters frequent vortex breakdowns. An other set-up providing stronger stretching has been to force it in a rotating tank by pumping the fluid out of the cell through a centred hole (Mory and Yurchenko 1993) or by injecting some air bubbles which rise along the axis of the cell (Turner 1966). However in these configurations the vortex is superimposed to a strong solid body rotation. An alternative set-up is proposed here, the circulation being provided by a rotating disk and the stretching artificially enhanced by pumping the fluid through a centred hole on top of the cell. This experimental configuration has already been used by Andreotti et al. (1997) to investigate the interaction between stretching and vorticity in such a vortex.

The experimental set-up is described in Sect. 2. The averaged velocity profiles are presented and discussed in Sect. 3.1 and 3.2. The influence of vortex precession and of particles concentration on these measurements is discussed and modelled in Sect. 3.3 and 3.4.

2 Experimental apparatus

2.1 Set-up

A stretched vortex is generated in a transparent altuglas cylindrical cell of 140 mm in diameter and 100 mm in depth,

Received: *5 August 1998/Accepted*: *20 February 1999*

R. Wunenburger
I.C.M.C.B, avenue Docteur A. Schweitzer
F-33608 Pessac Cedex, France

B. Andreotti
L.P.S., 24 rue Lhomond, F-75231 Paris Cedex 05, France

P. Petitjeans
L.P.M.M.H., 10 rue Vauquelin, F-75231 Paris Cedex 05, France

Correspondence to: B. Andreotti

We would like to thank J. E. Wesfreid, S. Douady and Y. Couder for very useful discussions. This work benefited from the support of CNRS.

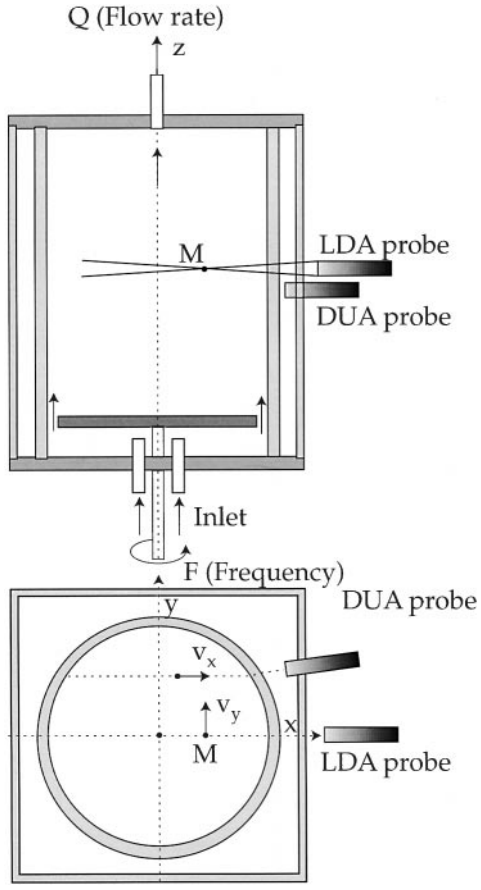

Fig. 1. Experimental set-up

shown schematically in Fig. 1. The cell is embedded in a square altuglas container with a side length of 190 mm. The space limited by the cylindrical and the plane boundaries is filled with water in order to avoid optical and ultrasonic bias.

On the bottom side of the cell a rotating disk (120 mm in diameter) sets the water into rotation. This disk is driven by a *DC* motor whose frequency F is adjustable up to 25 Hz. The water is sucked up through a hole of 12 mm in diameter positioned in the tank axis, opposite to the disk. It is then reinjected into the tank, via a reservoir, through holes symmetrically located behind the disk (Fig. 1). The flow rate Q is controlled with a peristaltic pump and can be adjusted up to a maximum of 2 L/min.

All the measurements presented here are performed at a flow rate $Q = 1.4$ L/min, and a frequency $F = 10$ Hz.

2.2 Velocity measurements

Two types of anemometers are used for this study: a laser Doppler anemometer (LDA) and a Doppler ultrasonic anemometer (DUA). The LDA apparatus uses a 80 mW laser Argon source ILT, a Bragg cell controlled by an AC 40 MHz generator and a PC-driven self-correlator TSI. It allows to measure one velocity component at a given point of the flow. The spatial resolution is of the order of 2 mm lengthways and 0.1 mm crossing. In order to obtain a velocity profile, the optical probe which combines the two laser beams is mounted on a micrometric displacement table so that the measurement volume M can be moved along the laser beam axis (Fig. 1). All measurements are performed at half depth, with horizontal Cartesian coordinates (x, y) centred on the vortex axis, (Ox) being parallel to the laser beam. The distance y_M between the laser beam and the axis of rotation of the disk, which is identical to the precession axis and to the mean position of the vortex core, remains constant during the whole measurement of a velocity profile. In order to simplify the velocity data analysis, y_M should be equal to zero for LDA, whereas for DUA y_M should be larger than the precession radius. To determine the position of the central axis, air bubbles are introduced in the reservoir above the reinjection tube. They are trapped inside the vortex core where they stay a sufficiently long time to coalesce and to form an air column. This thin column helps in visualizing the vortex axis. In order to get free of geometrical defects of the tank that could have shifted the axis of rotation of the disk from the tank axis, the mean position of the precessing vortex core is determined by analysing successive pictures of the air column together with the laser beam. Its mean position corresponds to the precession axis. y_M can be then adjusted to be as small as possible (smaller than 0.5 mm) and is kept constant during the whole measurement of a radial velocity profile. The orientation of the laser beams is chosen to measure the transverse velocity component v_y (Fig. 1). In the particular case studied here, the radial velocity ($v_r \sim 1$ mm/s) is negligible compared to the tangential one ($v_\theta \sim 1$ m/s). v_y and v_θ are thus directly linked by:

$$v_y(x, y) = \frac{x}{\sqrt{x^2+y^2}}\, v_\theta\left(\sqrt{x^2+y^2}\right) \tag{1}$$

so that the tangential component is directly measured ($v_y = v_\theta$) if $y = 0$.

There is a strong advantage using DUA rather than LDA: it allows to measure quasi instantaneously the profile, along the axis (Ox) of the probe, of the longitudinal velocity component v_x (Fig. 1). The DUA anemometer, type DOP 1000/628BS, allows, with a 4 MHz probe, to measure velocities up to about 4m /s by steps of 5 mm/s. One profile consists of 114 points of measurements separated by 0.75 mm along the axis Ox. A sequence of 1024 profiles equally spaced by 0.0375 s is measured in each record. Here, v_x is related to v_θ by

$$v_x(x, y) = \frac{-y}{\sqrt{x^2+y^2}}\, v_\theta\left(\sqrt{x^2+y^2}\right) \tag{2}$$

The main consequence of this relation is the difficulty of accessing the details of the vortex core since v_x tends to zero at the centre.

2.3 Tracers concentration measurements

Both for LDA and DUA, the tracers are TiO_2 particles whose characteristic size is 1 μm and whose density d is slightly larger than one ($d = 1.05$). In the stationary state, the concentration field is measured with a CCD camera, the particles being illuminated with a plane of laser light (in the radial plane (Oxz)). Assuming that for sufficiently low concentrations, light absorption by the foreground particles is negligible, the intensity

received by the camera is directly proportional to the concentration $C(x, z)$.

We observe in Fig. 2 that a tubular region of high concentration surrounding a central dark column nearly empty of particles is formed. This phenomenon of inhomogeneous concentration of solid particles has already been observed by Hasinger (1968). This surprising behaviour will be analysed in details in a further article. The particles concentrate after a typical timescale much larger than the characteristic hydrodynamical time scale ($1/F$), and in fact follow the flow streamlines at roughly the same velocity as the surrounding fluid, behaving commonly as lagrangian tracers from the point of view of velocimetry.

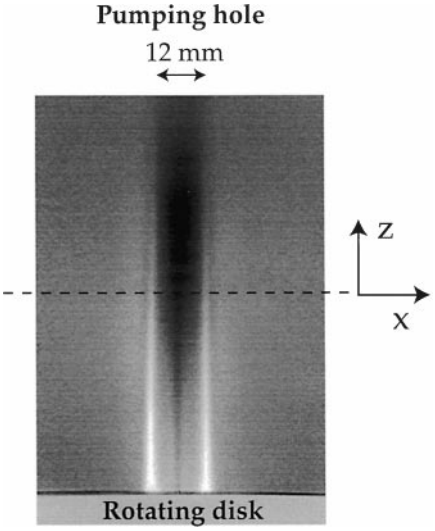

Fig. 2. Intensity diffused by the TiO_2 tracers enlightened by a laser sheet in the radial plane ($0\,x\,z$). Theparticles appear to demix from a central column (in black) to concentrate in a tubular region around it (in white)

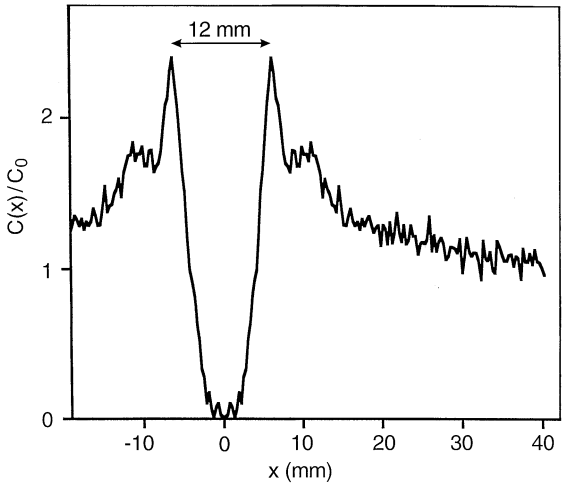

Fig. 3. Radial profile of the tracers concentration $C(r)$ at half-height of the cell. C_0 is the uniform concentration measured when there is no flow.

We measured the radial profile $C(x)$ of the concentration at half-height of the cell (Fig. 3). It is roughly parabolic in the central column, exhibits a sharp maximum for $x \sim 6.3$ mm and then decreases toward the mean concentration C_0.

3
Characterisation of the vortex

3.1
Averaged velocity profile using LDA technique

In order to obtain a satisfactory spatial resolution in the vortex core, the distance between two consecutive measurement points is chosen to be 0.33 mm. Unfortunately the counting rate is not sufficient to get a continuous sampling: the only available information is thus the probability distribution function $P(v_y; x_M)$ of the v_y velocity component at each point x_M, estimated here on 10000 Doppler bursts.

In order to get an idea of the tangential velocity profile $v_\theta(r)$, we first compute the average profile $\langle v_y(x_M)\rangle$ and the corresponding standard deviation (Fig. 4). The main features of this averaged velocity profile are those of a strong concentrated vortex superimposed on a residual solid body rotation: the tangential velocity increases in a thin core and has a decreasing tail around it. We choose to fit it with the sum of a Burgers' vortex velocity profile (Burgers 1940) and of a residual solid body rotation, as already proposed by Escudier et al. (1982) for velocity profiles of confined vorticies:

$$v_\theta(r) = \frac{\Gamma}{2\pi r}\left(1 - \exp\left(\frac{-r^2}{2\lambda^2}\right)\right) + \frac{1}{2}\,\omega r \qquad (3)$$

The best fit is shown in Fig. 4a, together with the experimental data. It can be seen that the agreement between the model curve and the experimental data is quite good. The interest of this fit is not really to compare the laboratory vortex to a Burgers' vortex, but to characterize it by few parameters which have clear physical meaning: Γ is the circulation of the vortex core, λ is the characteristic size of the core and ω corresponds to a residual vorticity enhanced by the rotating disk. The best fit is obtained for $\Gamma = 0.0704$ m^2/s, $\omega = 14.7$ Hz and $\lambda = 3.96$ mm. It is worth noting that the Reynolds number based on the circulation is very large ($Re \sim 10^5$) but the flow is apparently not turbulent. A complete discussion on turbulence depletion in a vortex can be found in a previous article (Andreotti et al. 1998).

There should be no problem in the determination of Γ and ω which are derived essentially from the velocity profile outside the core i.e. in a region where the standard deviation is small (Fig. 4a). On the other hand, the measurement dispersion strongly increases inside the vortex core. This is confirmed in Fig. 4b by the shape of the velocity PDFs $P(v_y; x_M)$, plotted in grayscale as a function of x_M and v_y. The velocity PDF at one point of measurement x_M corresponds to a vertical cut of Fig. 4b, the maximum of probability being conventionally represented by the black color. The best fit curve based on Eq. (3) is globally inside the high probability region of the PDF, but the vertical width of this region strongly increases in the vortex core. As a consequence, the details of the vortex core structure could be mistaken by taking the averaged profile. The effects responsible of this increased measurement dispersion are discussed in details in Sect. 3.4.

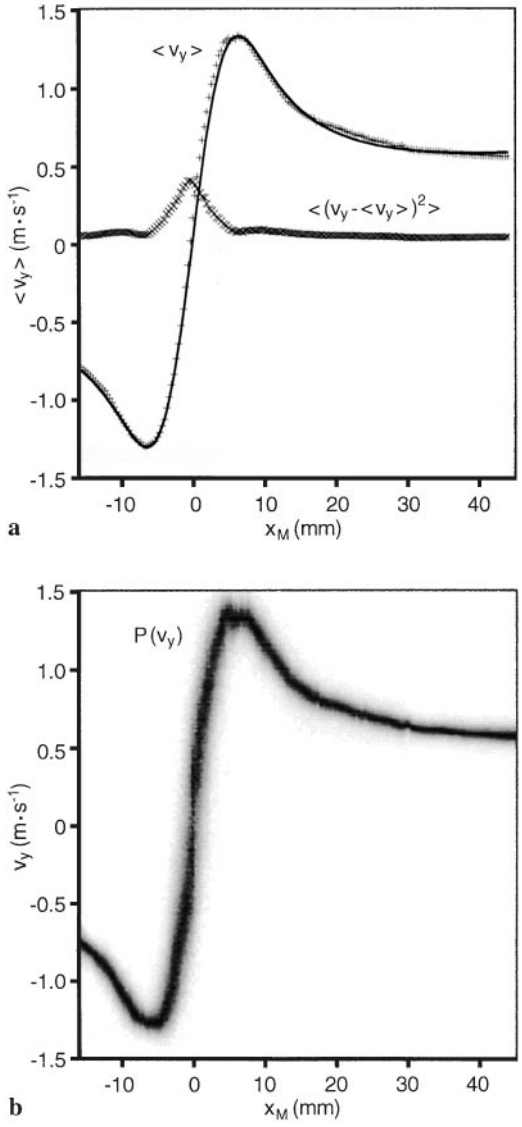

Fig. 4. a Velocity profile $\langle v_y(x_M)\rangle$ measured by averaging LDA measurements, and the corresponding variance $\langle v_y^2 - \langle v_y\rangle^2\rangle$. The solid line is the fit by the sum of a Burgers' vortex profile and a residual solid body rotation. **b** PDFs of the LDA measurements $P(v_y; x_M)$ as functions of the velocity v_y and of the position x_M. For each measurement point x_M, the PDF maximum appears in black

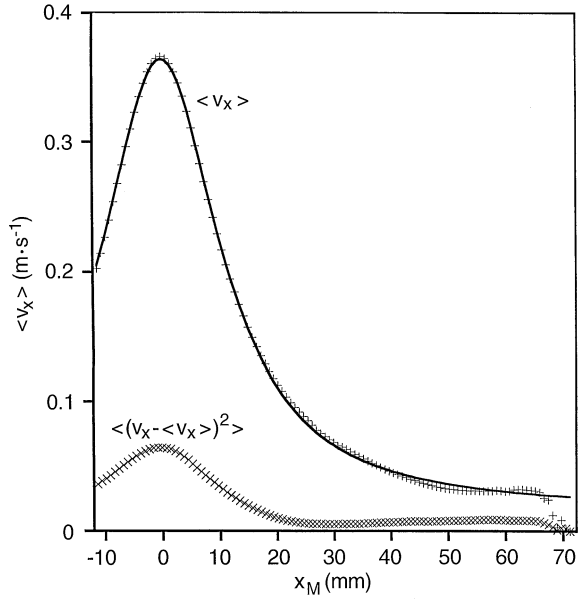

Fig. 5. Velocity profile $\langle v_x(x_M)\rangle$ measured by averaging DUA measurements, and the corresponding variance $\langle v_x^2 - \langle v_x\rangle^2\rangle$. The solid line is the fit by the sum of a Lorentzian, which corresponds to the projection of $1/r$ velocity profile, and a constant, which corresponds to a residual solid body rotation.

3.2
Averaged velocity profile using DUA technique

The DUA velocity measurements are performed at a distance y_M from the centre approximately equal to 12 mm. The velocity profile is therefore measured outside the vortex core. As for the LDA measurements, we compute the mean velocity profile $\langle v_x(x_M)\rangle$ and the corresponding standard deviation (Fig. 5). It must be emphasised that DUA is not sensitive to the local concentration of diffusing tracers, so that the averaged profile is an exact average in time contrary to LDA, whose statistics depend on the bursts frequency.

Outside the vortex core, Eqs. (2) and (3) simplify in

$$v_\theta(r) = \frac{\Gamma}{r} + \omega r \tag{4}$$

$$v_x(x, y) = -\frac{\Gamma y}{x^2 + y^2} - \omega y \tag{5}$$

The experimental points are shown together with the fit curve in Fig. 5. The best fit based on Eq. (4) is obtained for $\Gamma = 0.0760$ m^2/s, $\omega = 12.2$ rad/s and $y_M = 11.9$ mm. The difference between these values and those obtained by LDA are respective 8% for Γ and 20% for ω. However, the DUA method seems to be more adapted than LDA to the determination of the main characteristics of the vortex since the projection of the velocity on x axis (Equ. (2)) allows to separate clearly the residual solid body rotation (term independent of x of Eq. (5)) from the $1/r$ tail (Lorentzian function of x in Eq. (5)). Moreover, the standard deviation is smaller with DUA than with LDA. As for LDA measurement, the simple shape of the velocity profile allows to obtain good results simply by fitting the averaged velocity profile $\langle v_x(x_M)\rangle$ with the model one (5). We will show in the next section that this simplification allows to determine the position of the vortex centre as a function of time.

3.3
Influence of the vortex precession on DUA measurement

Consider a simple model of precession (Fig. 6) in which the vortex centre C(x_C, y_C) turns around the cell's axis on a circular trajectory of radius δ:

$$x = x_M - x_C = x_M - \delta\cos\theta \tag{6}$$

$$y = y_M - y_C = y_M - \delta\sin\theta \tag{7}$$

We assume for simplicity that both the angular velocity $\dot{\theta}$ and the radius of precession δ are constant with time, that the flow is stationary in the vortex frame of reference and that the tangential velocity v_θ is large compared to the velocity of the vortex centre $\delta\dot{\theta}$. The velocity measured at point M is still given by Eq. (2), using however x and y defined by Eqs. (6) and (7). The model velocity profile results from Eq. (5) and shows a very interesting analytical property: its average in time is strictly equal to the instantaneous profile in the vortex frame of reference. Outside the vortex core, the influence of the precession should thus be negligible. This allows to get more information from the measurements. Indeed, each instantaneous velocity profile can be fitted in the same way than the averaged profile (Eqs. (5)–(7)). The only problem comes from the large number of parameters to be fitted, together with the dispersion of the data. However, if the values previously obtained for Γ, ω and y_M (see Sect. 3.2) are imposed, only two free parameters remain to be adjusted on each profile: x_C and y_C, the coordinates of the vortex centre. The resulting curves $x_C(t)$ and $y_C(t)$ are shown in Fig. 7a. They appear to oscillate in phase quadrature, with a frequency 2.2Hz. The corresponding trajectory of the vortex centre is shown on Fig. 7b. It is roughly circular and the radius of precession δ is around 4 mm. As assumed above, δ varies more slowly than θ. Moreover the value of δ is in good agreement with the direct observation of the vortex axis motion using air bubbles. These measurements validate the precession model, which is used in the next section to discuss LDA measurements.

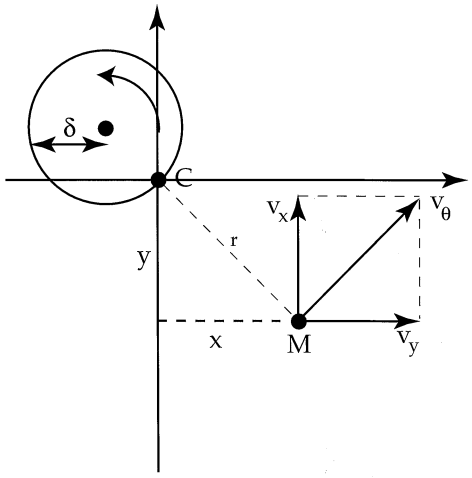

Fig. 6. Sketch of the vortex precession

3.4
Influence of the vortex precession on the LDA measurements

Let us consider a velocity histogram inside the vortex core measured at $x_M \sim -0.66$ mm (Fig. 8a). It can first be compared to the PDF which would have been obtained in the absence of perturbing effects. By taking into account only the intrinsic dispersion of the measurements, the probability of measuring a velocity v given the real velocity v_o is approximately Gaussian:

$$P(v) = \frac{1}{\sqrt{2\pi\sigma^2}} \exp\left(-\frac{(v - v_o)^2}{2\sigma^2} \right) \tag{8}$$

The variance σ, measured for a uniform steady flow, is equal to $\sigma_o \simeq 35$ mm/s. This ideal PDF is plotted together with the experimental one on Fig. 8a, using v_o as the averaged velocity. The measurement dispersion is obviously far from the ideal error distribution.

As a consequence, we should take into account the precession of the vortex, following the same analysis as in Sect. 3.3. Assuming that $y_M = 0$, Eq. (7) reduces to $y = -\delta\sin(\theta)$ so that the distance r between the measurement point M and the

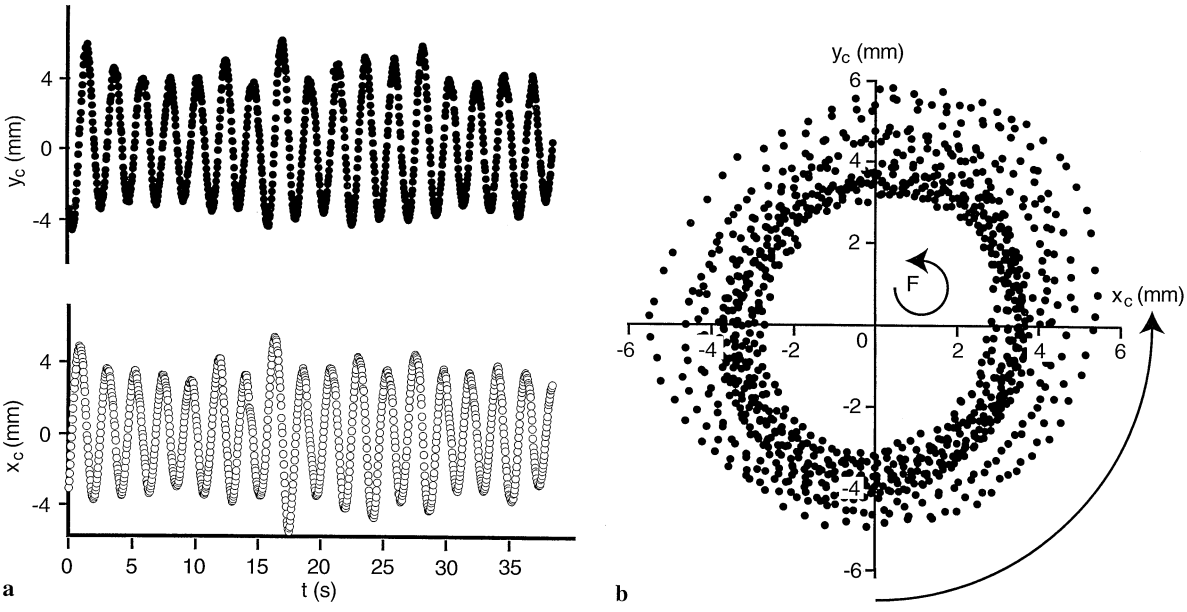

Fig. 7a,b. Position of the vortex centre (x_C, y_C) deduced from the fit of the instantaneous velocity profiles $v_x(x_M, t)$ measured with DUA. **a** Coordinates as functions of time; **b** vortex centre trajectory

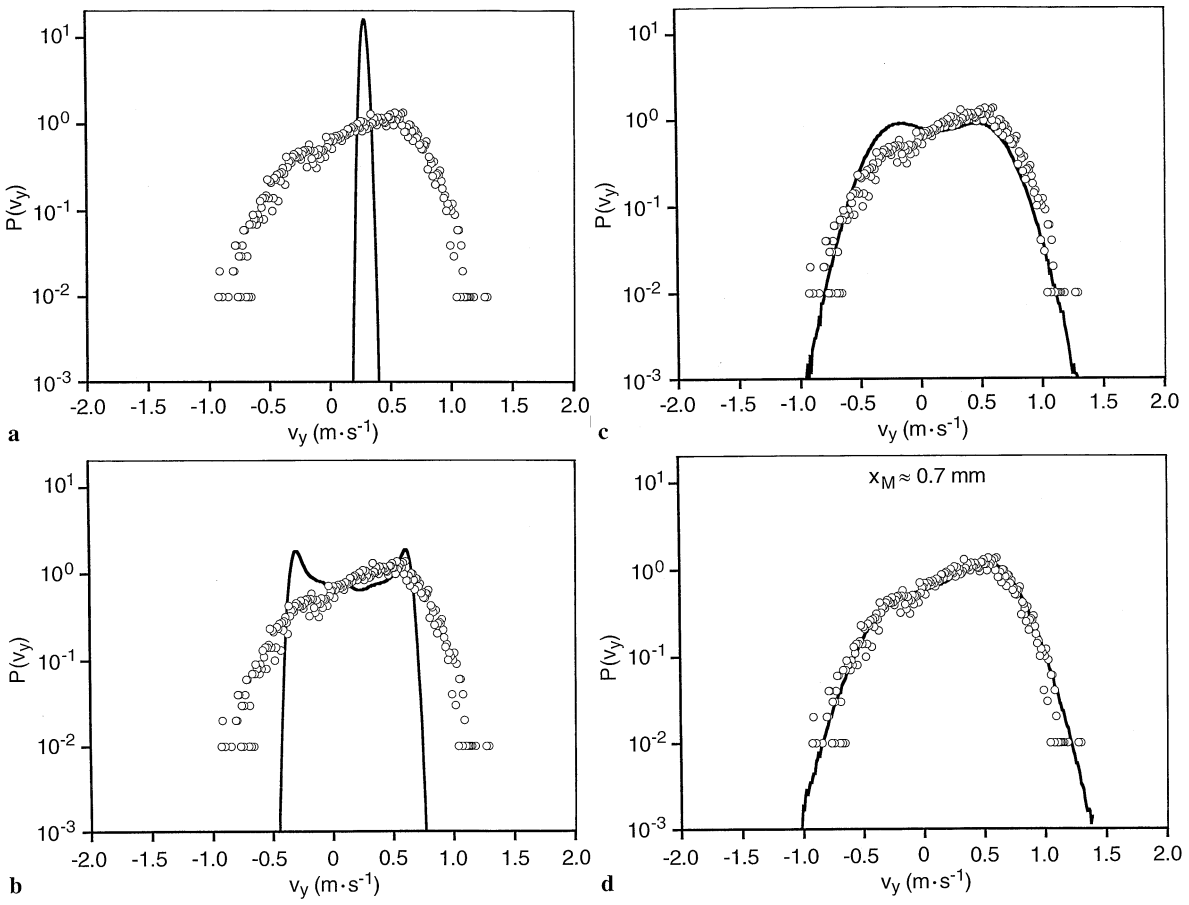

Fig. 8a–d. Experimental PDF of the velocity measured by LDA, for $x_M \simeq 0.7$ mm (circles) compared to (solid line). **a** The Gaussian distribution observed for a uniform flow; **b** the PDF obtained taking also into account the slight vortex precession; **c** that obtained with a dispersion enhanced by the strong velocity gradient **d** the PDF computed with the vortex precession, the large dispersion but also the variation of the counting rate due to the tracers demixion

vortex centre C is given by

$$r^2 = x^2 + y^2 = {x_M}^2 + \delta^2 - 2\delta x_M \cos\theta \tag{9}$$

All the values of the angle θ have same probabilities of occurence. Ignoring momentarily the intrinsic dispersion, the velocity PDF $P(v)$ is then simply proportional to the inverse of the derivative of v_y towards θ. It should have two maxima corresponding to the angles $\theta = 0$ and $\theta = \pi$, i.e. to the "apogee" and the "perigee" of the vortex trajectory. Using the expression of the velocity derived from Eqs. (1), (6), (7) and (9), it can easily be shown that these maxima are approximately separated by

$$v_y(\pi) - v_y(0) \simeq 2\delta \frac{\partial v_\theta}{\partial r} \tag{10}$$

The fluid motion in the vortex core is to the first order in r a solid body rotation ($v_\theta(r) = \Omega r$). In this particular case, the PDF can be exactly computed

$$P(v) = \frac{1}{\pi\sqrt{(\Omega\delta)^2 - (v - \Omega x_m)^2}} \tag{11}$$

It diverges and has a maximum for $v = \Omega(x_m \pm \delta)$.

We can now take into account the effect of both the intrinsic measurement dispersion and the precession on the probability distribution function. It is plotted in Fig. 8b, using the vortex model (3) with the values of the parameters determined in the previous sections. As predicted (11), the model PDF is now larger and shows two maxima smoothed by the Gaussian dispersion (8). However, the experimental PDF presents only one maximum and is even smoother. Therefore we have to take into account further effects.

The low spatial resolution (about 2 mm lengthways) should have an influence on the variance σ since it allows large velocity differences inside the measurement volume. It can be shown that, to the first order, the intrinsic variance σ depends in a quadratic way on the velocity gradient along the measurement volume:

$$\sigma^2 = \sigma_o^2 + a^2 \left(\frac{\partial v_y}{\partial x}(x, y) \right)^2 \tag{12}$$

where a is the effective spatial resolution ($a \sim 0.5$ mm). With this dependence of σ on the velocity derivative, the model PDF becomes as large as the experimental one (Fig. 8c) but the two maxima remain symmetric around the mean value.

The only effect which can explain the symmetry breaking between the two maxima is the fluctuation of the counting rate. As a matter of fact the experimental PDF corresponds to a probability in Doppler bursts and not straightforwardly to a probability in time. In our case, the counting rate varies by a factor 1000 from the vortex axis to its periphery. The counting rate is proportional to the tracers velocity and to their concentration. Due to the fact that the Bragg cell shifts all the velocities by 10 m s^{-1}, the measured velocities differ weakly from place to place and so the influence of the velocity gradients on the counting rate can be neglected. Then the main cause for the spatial variation of the counting rate is the spatial variation of the concentration in particles $C(r)$. Including an instantaneous counting rate proportional to the local concentration, the velocity PDF becomes:

$$P(v; x_M) \propto \int_{-\pi}^{\pi} C(r) \frac{\exp(-(v - v_y(x, y))^2/2\sigma^2)}{\sigma|(dv_y(x, y)/d\theta)|} d\theta \qquad (13)$$

where x, y, r and σ implicitly depend on θ (Eqs. (6), (7), (9) and (12)). We performed a numerical integration of this PDF formula, adjusting the core size λ to obtain the best fit of the experimental histograms. We used for Γ, ω and δ the values found with DUA. As before, the model PDF is shown for $x_M \sim -0.66$ mm on Fig. 8d. It is now both qualitatively and quantitatively similar to the experimental one. In particular, the symmetry between the apogee and the perigee of the vortex trajectory is broken due to the spatial inhomogeneity of the tracers concentration.

In conclusion, the increased measurement dispersion in the vortex core can be ascribed to three causes: a slight precession of the vortex, the inhomogeneity of the tracers concentration which induces fluctuations of the counting rate and the intrinsic dispersion of the measurements. To clarify their effects, it is interesting to see how the PDF evolve from place to place. In the centre of the cell, for $x_M \sim 0$ (Fig. 9a and b), the PDF exhibits two symmetric maxima. This is the signature of the vortex precession. For $x_M \sim 1$ mm (Fig. 10a and b), the maximum of the PDF corresponding to the lowest velocity disappears and is replaced by a large probability tail. The PDF for $x_M \sim 0.7$ mm (Fig. 8d) is an intermediate case where the second maximum is weakened but still visible. The main reason for these differences is the large probability of detecting a Doppler burst in a region where particles are concentrated (in the periphery of the vortex (Figs. 2 and 3)). As a consequence the difference between Figs. 9 and 10 is mainly due to the low tracers concentration inside the vortex core. Finally, at $x_M \sim 4.3$ mm (Fig. 11a and b), the measurement point is close to the mean positions of both the maximum of the tracers concentration and the velocity maximum so that the velocity PDF is very sharp. The difference between the curvatures of the tails of the velocity PDFs measured at $x_M \sim 0$ and at $x_M \sim 4.3$ mm can only be explained by an increased dispersion of the velocity measurements at $x_M = 0$ due to the large velocity gradient near the vortex axis. The effect of the inhomogeneity of the tracers concentration is not only to break the symmetry between the probability maxima of the PDF, but also to shift the mean velocity and the most probable velocity. In this particuliar flow, the gradients of the tracers concentration make the measurement of high velocities much more probable than that of low velocities. Consequently the mean velocities

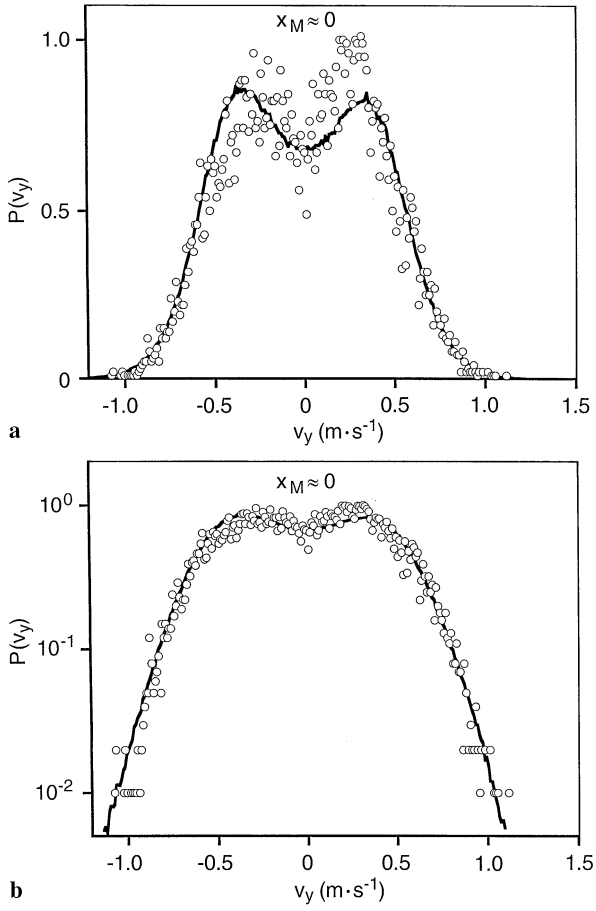

Fig. 9a,b. Experimental (circles) and model (solid line) PDFs of the velocity measured by LDA in the centre of the cell ($x_M \simeq 0$) **a** in linear representation and **b** in semi-logarithmic one. The PDF exhibits two symmetric maxima due to the vortex precession

in the vortex core are over estimated. Considering the PDF measured at $x_M \sim 4.3$ mm for instance, the real velocity in the vortex frame of reference is slightly lower than the most probable value (-1.22 m/s instead of -1.29 m/s). This shifting effect is confirmed by considering the value of the core size $\lambda = 4.31$ mm found by fitting the experimental histograms, which is 9% larger than the value obtained by fitting the average velocity profile (Fig. 4).

4 Conclusion

Some experimental problems of velocity measurement in a precessing laboratory vortex were discussed. The measurement dispersion in instantaneous DUA profiles leads to a loss of the temporal information on the precession motion of the vortex. However this information can be restored using a simple model in which the flow is assumed to be steady in the vortex frame of reference. The averaged velocity profile is then sufficient to characterise this flow and the coordinates of the vortex can be deduced by fitting the instantaneous profiles. LDA measurements appear to be more problematic since the precession and the spatial variations of tracers concentration lead to strong fluctuations of the velocity. However the whole

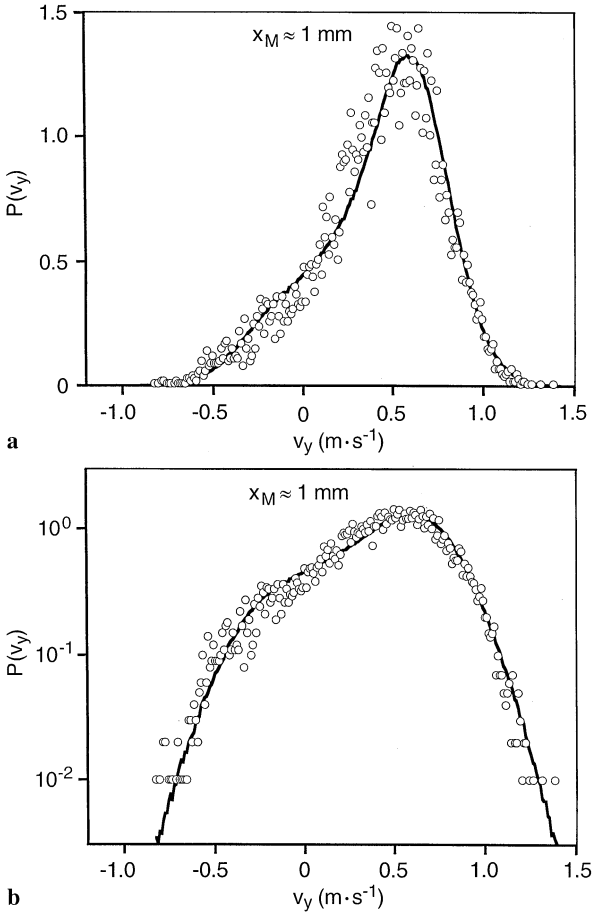

Fig. 10a,b. Same as Fig. 9 but for $x_M \simeq 1$ mm. The low velocity probability maximum is weakened due to the variationof the concentration in tracers

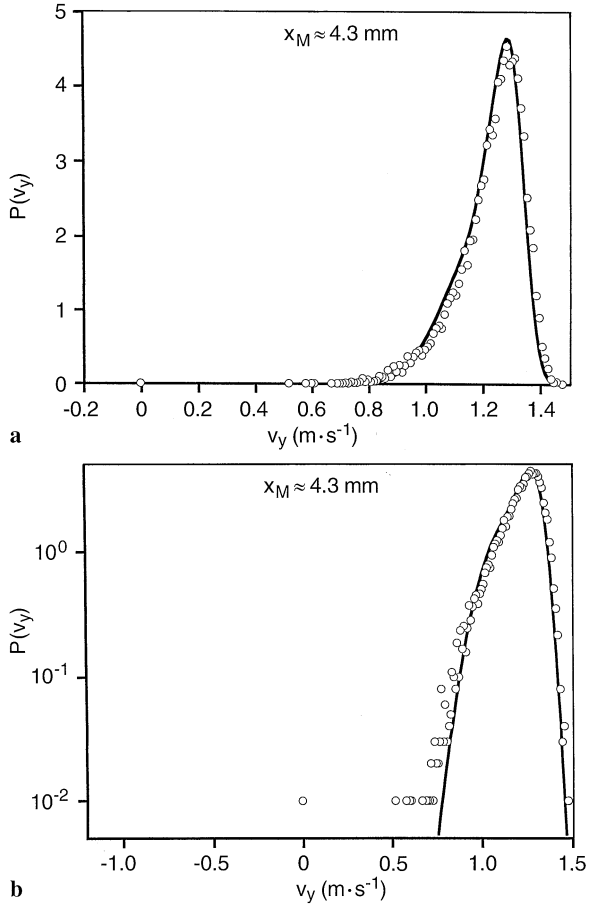

Fig. 11a,b. Same as Fig. 9 but for $x_M \simeq 4.3$ mm. The velocity PDF becomes sharp both because the velocity gradient is lower and because of the large concentration in particles

information about the flow can be recovered through the study of the one point velocity PDFs.

As a conclusion, we want to stress the fact that a measurement histogram contains much more information than a simple average. For instance, the measurement dispersion appears to be non-Gaussian in many experimental situations and a complete study of the dispersive effects can then improve the measurements.

References

Andreotti B; Douady S; Couder Y (1997) About the interaction between vorticity and stretching in coherent structures. In: Turbulence modelling and vortex dynamics, eds O Boratav, A Eden, A Erzan, pp. 92–107. Springer, Berlin

Andreotti B; Maurer J; Couder Y; Douady S (1998) Experimental investigation of turbulence near a large scale vortex. Eur J Mech B 17: 451–470

Burgers JM (1940) Application of a model system to illustrate some points of the statistical theory of free turbulence. Proc Acad Sci Amsterdam 43: 2–12

Escudier MP; Bornstein J; Maxworthy T (1982) The dynamics of confined vortices. Proc. R. Soc. Lond. 382: 335–360

Escudier MP (1984) Observations of the flow produced in a cylindrical container by a rotating endwall. Exp Fluids 2: 189–196

Hasinger SH (1968) An experiment with particles in a free vortex. AIAA J 6: 939–940

Mory M; Yurchenko N (1993) Vortex generation by suction in a rotating tank. Eur. J Mech B/Fluids 12: 729–747

Mory M; Spohn A (1992) Vortex flow generated by a rotating disc. In: Rotating fluids in geophysical and industrial applications, pp. 301–312. Springer, Berlin

Pinton JF; Labbe R (1994) Correction to the Taylor hypothesis in swirling flows. J Phys II 4: 1461–1468

Turner JS (1966) The constraints imposed on tornado-like vortices by the top and bottom boundary conditions. J Fluid Mech 25: 377–400